

# Search for pulsation among suspected A-type binaries and the new multiperiodic $\delta$ Scuti star HD 217860<sup>★</sup>

Y. Frémat<sup>1</sup>, P. Lampens<sup>1</sup>, P. Van Cauteren<sup>2</sup>, S. Kleidis<sup>3</sup>, K. Gazeas<sup>4</sup>, P. Niarchos<sup>4</sup>,  
C. Neiner<sup>5</sup>, D. Dimitrov<sup>6</sup>, J. Cuypers<sup>1</sup>, J. Montalbán<sup>7</sup>, P. De Cat<sup>1</sup>, and C.W. Robertson<sup>8</sup>

<sup>1</sup> Royal Observatory of Belgium, 3 avenue circulaire, 1180 Brussel, Belgium

e-mail: yves.fremat@oma.be

e-mail: patricia.lampens@oma.be

<sup>2</sup> Beersel Hills Observatory, Beersel, Belgium

<sup>3</sup> Zagori Observatory, Epirus, Greece

<sup>4</sup> University of Athens, Department of Astrophysics, Astronomy and Mechanics Panepistimiopolis, 157 84, Zografos, Athens, Greece

<sup>5</sup> GEPI / UMR 8111 du CNRS, Observatoire de Paris-Meudon, 5 place Jules Janssen, 92195 Meudon, France

<sup>6</sup> Institute of Astronomy, Bulgarian Academy of Sciences, 72 Tsarigradsko Shosse Blvd., 1784 Sofia, Bulgaria

<sup>7</sup> Université de Liège, Institut d'Astrophysique et de Gophysique, Alle du 6 Aot, 17 Sart Tilman, Liège, Belgium

<sup>8</sup> SETEC Observatory, Goddard, Kansas, USA

Preprint online version: September 5, 2021

## ABSTRACT

**Context.** In the H-R diagram, the intersection of the main sequence and the classical Cepheid instability strip corresponds to a domain where a rich variety of atmospheric phenomena are at play (including pulsation, radiative diffusion, convection). Main-sequence A-type stars are among the best candidates to study the complex interplay between these various phenomena.

**Aims.** We have explored a sample of suspected A-type binaries in a systematic way, both spectroscopically and photometrically. The sample consists of main-sequence A-type stars for which the few existing radial velocity measurements may show variability, but for which other essential information is lacking. Due to their location in the H-R diagram, indications of pulsation and/or chemical peculiarities among these suspected binary (or multiple) systems may be found.

**Methods.** High-resolution spectroscopy obtained with the ELODIE and MUSICOS spectrographs was used in combination with a few nights of differential CCD photometry in order to search for pulsation(s). In order to search as well for chemical peculiarities or for possible hidden component(s), we derived the atmospheric stellar parameters by fitting the observed spectra with LTE synthetic ones.

**Results.** Of the 32 investigated targets, eight are spectroscopic binaries, one of which is a close binary also showing eclipses, and three have been identified as  $\delta$  Scuti pulsators with rapid line-profile variations.

**Conclusions.** Among the latter stars, HD 217860 reveals interesting multiperiodic photometric and spectroscopic variations, with up to eight frequencies common to two large photometric data sets. We suggest that at least one radial overtone mode is excited among the two most dominant frequencies, on the basis of the computation of the pulsation constants as well as of the predicted frequencies and the expected behaviour of the amplitude ratio and the phase difference in two passbands using adequate theoretical modelling. We furthermore found evidence for a strong modulation of the amplitude(s) and/or the (radial) frequency content of this intriguing  $\delta$  Scuti star.

**Key words.** Stars: binaries: spectroscopic – Stars: atmospheres – Stars: fundamental parameters – Stars: variables: general – Stars: oscillations –  $\delta$  Sct

## 1. Introduction

In their catalogue of stellar radial velocities, Grenier et al. (1999) noticed that 32% of the sample of B8-F2 type stars observed by the Hipparcos satellite have variable velocities and assumed that this variability was due to multiplicity only.

Though this conclusion remains valid when performing statistics on the overall occurrence of multiplicity, it is realistic to think that some of the studied stars are also non-radial pulsators showing line profile variations (LPVs). In the H-R diagram, this situation may happen, for example, at the intersection of the classical Cepheid instability strip (CIS) and the main sequence (where the mid-A to early-F type stars are). In this region, a rich variety of phenomena are at play in the stellar atmospheres, some of which are expected to produce long- and/or short-term variability. These phenomena consist in the

<sup>★</sup> This work is based on spectroscopic observations made at the Haute-Provence Observatory (OHP), the Observatoire du Pic du Midi (TBL) and the Bulgarian National Astronomical Observatory (NAO, Rozhen).

different pulsation mechanisms (active in the  $\delta$  Scuti, SX Phe,  $\gamma$  Dor and roAp variable stars) and in various other processes involving magnetism, diffusion, rotation and convection. The latter processes may boost or on the contrary inhibit the presence of chemical peculiarities (occurring in Ap, Am,  $\rho$  Pup and  $\lambda$  Boo stars). The competition between these processes and mechanisms thus leads to a large mix of stellar groups of different atmospheric composition (Dworetzky 2004). These stellar groups also behave in different ways with respect to pulsation and binarity, resulting in non-symmetric spectral lines which can lead to misinterpretation of the radial velocity (RV) measurements.

Combining high-resolution spectroscopy and CCD photometry, the present work aims at exploring the RV variability of several poorly known HIPPARCOS targets located at the lower end of the instability strip. For one of the most promising targets (HD 217860) showing multiperiodic variations, we performed a frequency analysis of the multi-site differential photometric time series. The data and the reduction procedure are described in Sect. 2, while the tools and the procedure we adopted to derive the stellar parameters (effective temperature, surface gravity and projected rotational velocity) and their errors are described in Sect. 3. Section 4 and 5 provide respectively the global results and a discussion of several interesting targets. We present the conclusions and future perspectives of this project in Sect 6.

## 2. Observations and data reduction

### 2.1. Target selection

32 targets from the HIPPARCOS catalogue have been selected according to the following criteria : 1) brighter than magnitude 8; 2) spectral type ranging from A0 to F2; 3) showing some indication of radial velocity variability (Grenier et al. 1999); and 4) preferentially with less than ten references in the bibliography recorded in the SIMBAD database at the CDS. The selected targets are ordered by increasing HD number in Table 1, with the HIP number (col. 2), number of references in SIMBAD (col. 3), V magnitude (col. 4) and spectral type (col. 5) from Grenier et al. (1999).

### 2.2. High-resolution spectroscopy

The spectroscopic observations were carried out at the 1.93 m telescope of the OHP (Baranne et al. 1996), equipped with the ELODIE spectrograph (R~40000). High-resolution spectra were collected during 4 nights in 2004 (December 3–7). Each target was observed 2 to 5 times in order to be able to detect rapid (periods of order of a few hours) or slow (periods of the order of a few days) line profile variations (LPVs) and/or changes in radial velocity. However, due to the weather conditions, some of our targets have only been observed 2–3 consecutive times, without the possibility to reobserve them at a later date. We adapted the time exposures to ensure a S/N ratio per pixel usually varying from 70 to 100 (at 5000 Å). The journal of observations is given in Table 2 and contains: the HD identifier (col. 1), Heliocentric Julian Day (HJD, col. 2),

**Table 1.** Target description. Nref is the number of references in SIMBAD at present. The spectral type is from Grenier et al. (1999).

HD	HIP	Nref	V	Sp. Type
849	1043	7	7.17	A4 V
3066	2719	1	7.36	A3 V
3743	3165	7	7.21	A4 III
3777	3227	9	7.44	A2 III
5066	4129	12	6.70	A2 V
6813	5416	3	7.36	A2 IV
7551	5886	3	6.71	A3 V
11190	8581	1	7.88	A2 III
12389	9501	8	7.98	A4 V
12868	9851	3	7.25	A4 II
13162	10045	1	7.92	A2 IV
14155	10731	2	7.44	A3 V
17217	13063	2	6.92	A2 V
19257	14479	3	7.07	A9 III
20194	15177	3	7.92	A5 V
25021	18777	11	7.29	A2 V
26212	19436	4	7.36	A5 V
27464	20495	3	7.76	A7 IV–III
30468	22352	6	7.03	A2 IV
31489	22984	2	7.49	A4 V
38731	27525	2	7.92	A7 V
42173	29375	1	7.55	A5 V
44372	30287	1	7.77	A2 V
64934	38891	4	7.00	A5 V
68725	40361	11	6.94	F2 Ib*
81995	46642	2	7.35	A7 III
217860	113790	2	7.30	A8 III
221774	116321	1	7.38	A4 IV
223425	117479	3	7.07	A2 V
223672	117646	19	7.34	A6 V
224624	118276	7	7.20	A2 V
225125	300	1	7.45	A7 IV

\*: rather a chemically peculiar main-sequence star (cf. Tab. 7)

**Table 2.** Journal of spectroscopic observations at OHP, TBL and NAO. The complete table is available in the electronic version of the paper.

HD	HJD–2400000	S/N	exp. [s]	RV [km s <sup>-1</sup> ]	Obs.
849	53346.2338	137	1200	10.46±5.93	OHP
	53346.2493	143	1200	5.17±4.10	OHP
3066	53343.3515	59	644	-12.15±1.35	OHP
	53343.3818	70	1200	-1.75±2.86	OHP
	53344.3245	104	1200	2.68±4.17	OHP
	53344.3399	104	1200	-8.86±2.30	OHP
...					

signal-to-noise ratio (col. 3), exposure time (col. 4), as well as the instantaneous radial velocity (col. 5) and the observatory's acronym (col. 6).

The data have been automatically reduced order-by-order at the end of the night using the INTERTACOS pipeline. The first 50 echelle orders were merged using the overlapping re-

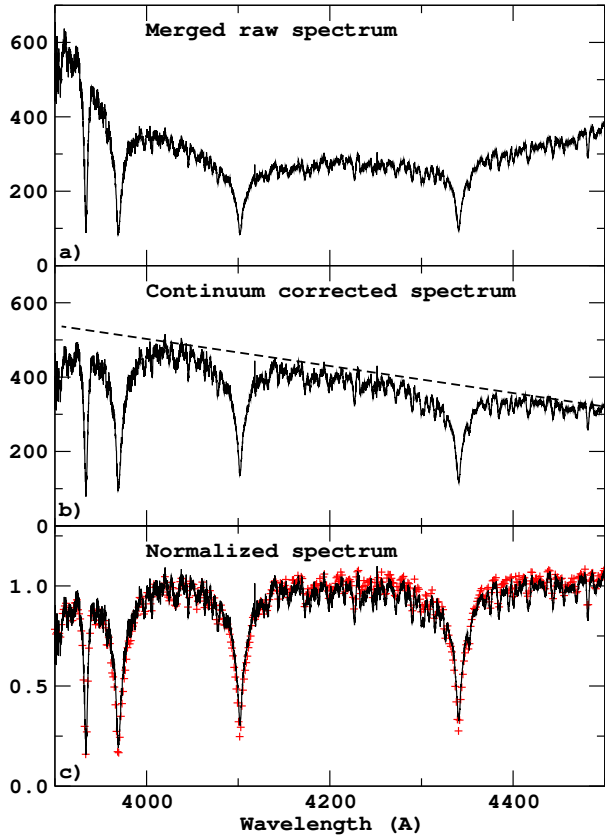


**Fig. 1.** Normalisation of the spectrum of HD 225125: a) Merged spectrum with incomplete removal of the instrumental signature/response; b) Corrected spectrum and continuum placement (broken line); c) Normalized observed spectrum (black line) compared to the synthetic one (red crosses).

gion and computing a ratio allowing to scale each order as described in Erspamer & North (2002). To ease normalisation of the spectra and to correct for the incomplete removal of the instrumental response (see Fig. 1a), we used the spectra of the stars in our sample with known Strömgren and  $H\beta$  colour indices. We adopted these indices to perform a first estimate of the stellar parameters and to compute a reference synthetic spectrum. An averaged function was obtained by dividing the observed data by this "reference spectrum", which was further used to correct the merged raw spectra (see Fig. 1b). Normalization was finally performed by fitting a line through the continuum between 4000 and 4500 Å with the CONTINUUM task of IRAF (see Fig. 1c).

To complete these data, some spectra were obtained with the MUSICOS spectropolarimeter (R~35000) mounted at the Cassegrain focus of the 2-m telescope Bernard Lyot Telescope (TBL) at the *Observatoire du Pic du Midi* (France) (Donati et al. 1999) in July 2005. The spectral domain covered ranges from 4500 to 6600 Å; these spectra were reduced with the ESPrIT software package developed by Donati et al. (1997) and improved by Neiner et al. (2003).

INTERTACOS and ESPrIT were also used to perform a cross-correlation of the observed spectra with the appropriate mask after each exposure. However, since most of our targets

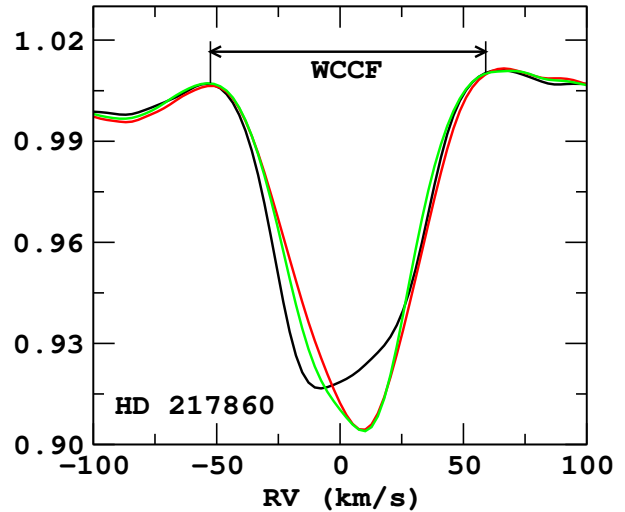


**Fig. 2.** The CCF of HD 217860 shown for 3 consecutive exposures.

have large  $V \sin i$  values, we recomputed the cross-correlation function (CCF) in a spectral domain ranging from 5000 to 5700 Å in order to avoid the hydrogen lines. Synthetic spectra obtained with the stellar parameters derived in Sect. 3.1 and for  $V \sin i = 0 \text{ km s}^{-1}$  were adopted as templates. An example of a CCF can be found in Fig. 2.

In two cases (HD 11190 and HD 68725), additional spectra were obtained with the Coudé spectrograph (with a resolution of  $0.19 \text{ Å/pixel}$ ) on the 2-m R-C telescope of the NAO Rozhen in December 2006. The spectral domain covers three regions from about 4440 to 4640 Å, from 6300 to 6500 Å, and around the  $H_\alpha$  line. These spectra were reduced with standard IRAF procedures. The corresponding radial velocities were measured with the cross-correlation technique using synthetic spectra.

### 2.3. CCD photometry

We additionally performed complementary and exploratory CCD photometry for the most promising targets of the sample, i.e. for those stars that showed interesting short-term variations of the CCFs, in the period between December 2004 and January 2006. This has not always been possible, however, as the targets are bright and suitable comparison stars were not always available in the used fields-of-view (FOVs). For this reason, various telescopes of different size have been used, including also very small instruments of only 13-cm aperture. Table 3 summarizes the technical specifications of these instruments. In some cases we had no other choice than to use the only other bright star in the field, even though the colour and/or magnitude difference was not optimal. Depending on the target's magnitude, a B or V filter according to Bessell's specifications (Bessell 1995) was employed.

The most promising candidates for short-term variability in the CCFs were submitted to two photometric runs of about half a night each in order to verify the presence of short-periodic light variations. Table 4 summarizes the journal of the observations for 7 of the 32 selected HIPPARCOS targets. In one

**Table 3.** Description of used instruments during the exploratory program. FOV (i.e. col. 4) stands for "Field Of View".

Observatory	Telescope	Camera	FOV	Notes
BHO	13-cm refractor	SBIG ST10XME	44'x29.5'	
	25-cm Newton	SBIG ST10XME	34'x23'	f/6
	40-cm Newton	SBIG ST10XME	26'x17.5'	f/5
HLO	12.5-cm refractor	SBIG ST10XME	40.5'x27.5'	guidescope of R-C tel.
HLO	1-m Cassegrain	Enzian	24'x12'	with focal reducer

**Table 4.** Journal of CCD photometric exploratory observations of the variable candidates. Observations were made at the Beersel Hills Observatory (BHO) and the Hoher List Observatory from the Argelander Institute for Astronomy, Bonn (HLO).

HIP	HD	Date	Observat.	Telescope Size	Filter	Time span (hours)	Remarks
3165	3743	12/13-Jan-05	BHO	13-cm	V	2	variable (with a periodicity of days ?)
		13/14-Jan-05	BHO	13-cm	V	2	shows a difference of 0.078 mag in mean light level
9501	12389	19/20-Dec-04	BHO	25-cm	V	4.8	previously known $\delta$ Scuti variable
15177	20194	10/11-Dec-05	HLO	12.5-cm	V	6.3	constant ( $\sigma=6$ mmag)
		14/15-Jan-06	BHO	25-cm	V	6	constant ( $\sigma=5$ mmag)
40361	68725	12/13-Jan-05	BHO	40-cm	B	7	new $\delta$ Scuti variable
		10/11-Dec-05	HLO	12.5-cm	B	5	
46642	81995	1/2-Apr-05	BHO	40-cm	B	6	partial eclipse; $\Delta m(\text{variable-check}) \approx 0.06$ mag
		10/11-Apr-05	BHO	40-cm	B	5.3	partial eclipse
		11/12-Apr-05	BHO	40-cm	B	4.8	constant ( $\sigma=4$ mmag)
113790	217860	3/19/20-Dec-04	BHO	40-cm	B	18.4	new $\delta$ Scuti variable
116321	221774	6/7-Feb-05	HLO	1-m	B	4.1	constant ( $\sigma=4$ mmag)
		14/15-Jan-06	BHO	40-cm	B	7	constant ( $\sigma=4$ mmag)

additional case (HD 30468), there was no suitable comparison stars in the field.

#### 2.4. Multi-site CCD photometry for HD 217860

HD 217860 was recognised by HIPPARCOS as a variable star but with an unsolved variability pattern (ESA 1997). Much to our surprise, a brief frequency-analysis of 113 selected measurements from the Hipparcos Epoch Photometry allowed us to detect a most dominant frequency at  $19.7474 d^{-1}$  with a significance ratio of about 10 (Hp-amplitude of 18 mmag), accompanied by a possible second frequency at  $14.2681 d^{-1}$  with a significance ratio between 5 and 6 (Hp-amplitude of 10 mmag). The variations in the light curves and the spectra are rapid (see Fig. 5 and also Frémat et al. 2006) and show the presence of multiple periods, confirming its status of  $\delta$  Scuti variable star. The light curves are sometimes very peculiar. We therefore collected CCD photometric (differential) data from various observatories equipped with small instruments in Europe, in the period between December 3, 2004 and December 25, 2005. The observations were carried out using a 0.4-m Newton equipped with a SBIG ST-10 XME CCD at Beersel Hills Observatory (BHO, Belgium), a 0.4-m reflector with a focal reducer and SBIG ST-8 CCD at the University of Athens Observatory (UAO, Athens, Greece), and a 20-cm telescope with a ST-7 XMEI CCD at Athens (ZO, Greece). We performed the observations using the B and V filters according to Bessell's specifications (Bessell 1995). Table 5 shows the details of the obser-

vational campaigns. Due to a technical problem, observations obtained at a fourth site could however not be used. We employed the software Mira AP<sup>1</sup> (vers. 6) to reduce the images following standard procedures (offset and dark current correction, flat-field calibration) and to compute the differential magnitudes using the technique of aperture photometry at BHO. At ZO and UAO, we used the package AIP4WIN (respectively the versions 1.4.21 and 1.4.25) (Berry & Burnell 2005).

All differential magnitudes have been computed using HIP 113918 (GSC 3997:1091) as the principal comparison star and GSC 3997:1078 as the check star. At BHO, additional comparison stars have been considered. In this case we identified GSC 3997:775 as NSV 14402 in the same field and also measured it. Since both HIP 113918 (the comparison star 'C1') and HIP 113790 (the variable star 'V') are much brighter than GSC 3997:1078 (the check star 'K'), the standard deviations of the mean differential magnitude in the sense (K - C1) are used as estimates of the highest noise level expected to be found in the residual data during the subsequent frequency analyses. We subtracted the overall averaged values for every measured star at each observatory. We initially also corrected for nightly shifts using the mean values of the differential magnitudes in the sense (K - C1) per night and per observatory. We next computed the relative weights of each time series by determining the night-to-night standard deviations of the (K - C1) differences, and we adopted a weight inversely proportional to their

<sup>1</sup> The Mira AP software is produced by Mirametrics Inc.

variance. The largest relative weight (set equal to 1) has been taken from the highest-quality time series. The preliminary analyses however showed that the corrections based on the (K - C1)'s nightly averages did not compensate well enough for the nightly shifts of the (V - C1) data in order to be able to remove most of the power in the low frequency regime. Therefore, we went one step further and corrected for nightly shifts using the mean values of the differential magnitudes in the sense (V - C1) per night and per observatory. In this way, we removed any signal that might indicate a real long-term periodical trend in the datasets. However, since our main interest is the study of the pulsations, we will only focus on the high-frequency regime from hereon.

### 3. Procedure and tools

We derived the fundamental stellar parameters ( $T_{\text{eff}}$ ,  $\log g$  and  $V \sin i$ ) by fitting our high-resolution spectra with synthetic ones (Sect. 3.1). For the double-lined spectroscopic binaries (SB2s) of our sample, the procedure was adapted to account for the existence of a companion and an additional parameter ( $R_{AB}^{\lambda}$ ), representing the monochromatic luminosity ratio between the components A and B, was defined (Sect. 3.2). The error bars for  $R_{AB}^{\lambda}$ ,  $V \sin i$  and  $T_{\text{eff}}$  represent the standard errors resulting from the different fitted zones, while those for  $\log g$  are derived from the uncertainties on the parallax (and on  $R_{AB}^{\lambda}$  for SB2s), on the one hand, and on the effective temperature, on the other hand.

#### 3.1. Stellar parameter determination: the general case

The radial velocity (RV), projected rotational velocity ( $V \sin i$ ), effective temperature ( $T_{\text{eff}}$ ), and surface gravity have been derived in four consecutive steps. First, the CCFs were used to estimate the instantaneous and averaged RV. Then, a comparison between observed and synthetic spectra allowed us to derive the projected rotational velocity and the effective temperature (Sect. 3.3). This has been performed by means of the GIRFIT computer code (Frémat et al. 2005b), which allows to conduct a least squares fitting based on the MINUIT minimization package. In this study, we mainly focused on several zones in the spectral domain ranging from 3900 to 4500 Å (Table 6), in which independent fits were performed. The determination of  $V \sin i$  is based on metallic line fitting with RV fixed and considering  $\log g$ ,  $T_{\text{eff}}$ , and  $V \sin i$  as free parameters. It is worth to remark that, at this stage, the procedure provides  $V \sin i$  only, while the values obtained for  $T_{\text{eff}}$  and  $\log g$  are not yet meaningful. Since most of the targets are cooler than 8500 K, the determination of  $T_{\text{eff}}$  was performed using the hydrogen lines as well as the Ca II K-line. This spectra-fitting procedure was completed adopting the previously obtained values of  $V \sin i$  and RV, while  $\log g$  was kept equal to 4.0 in the first iteration. The surface gravity has finally been derived by combining the HIPPARCOS parallax, V magnitude and  $T_{\text{eff}}$  value in order to estimate the stars' luminosity (Erspamer & North 2003). We then obtained the mass and radius from theoretical stellar evolutionary tracks computed for  $Z=0.02$  (Schaller et al. 1992). A

**Table 6.** Fitting zones used to derive the projected rotation velocity and effective temperature.

1. $V \sin i$ determination	
zone	line-type
4200 – 4230	Metals
4230 – 4260	Metals
4260 – 4290	Metals
4445 – 4460	Metals
4460 – 4475	Metals
4475 – 4487	Mg II
4485 – 4500	Metals
2. $T_{\text{eff}}$ determination	
zone	line-type
3915 – 3950	Ca II K-line
3950 – 4000	H $\epsilon$
4010 – 4200	H $\delta$
4200 – 4270	Metals
4270 – 4400	H $\gamma$
4450 – 4500	Metals

second iteration has been performed to test the sensitivity of the  $T_{\text{eff}}$  determination to a change in  $\log g$ .

#### 3.2. Stellar parameter determination in the case of SB2s

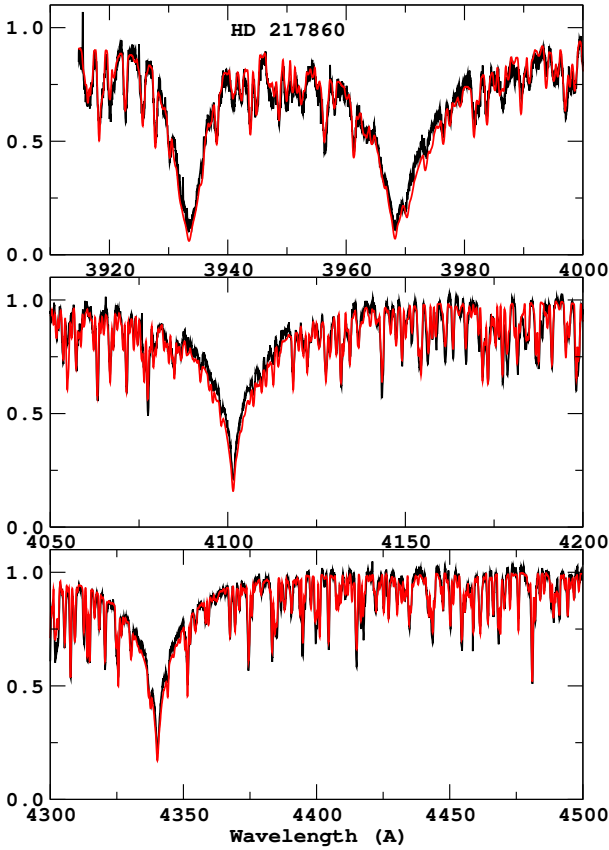
Stellar parameter determination of three SB2s of the sample (HD 6813, HD 11190, HD 221774) was carried out by enabling the GIRFIT programme to combine two wavelength shifted normalized synthetic spectra. In this version of the code, the input parameters are  $T_{\text{eff}}$ ,  $\log g$ ,  $V \sin i$ , and RV for each component. We further added a parameter representing the monochromatic luminosity ratio,  $R_{AB}^{\lambda} = L_{A,\lambda}/L_{B,\lambda}$ , between the components A and B of the system. RV and  $V \sin i$  values of each component have been derived in the same way as for single stars. In a first step, the effective temperature and the luminosity ratio of the stars have been fitted simultaneously, keeping the values of  $\log g$ , RV, and  $V \sin i$  fixed. The value of  $R_{AB}^{\lambda}$  is then used to estimate the components' V magnitude which, together with the parallax and the effective temperature, enables to derive the surface gravity (see Sect. 3.1). Where needed, several iterations were performed to get a coherent set of parameters.

#### 3.3. Model atmospheres and flux grid

In order to determine the stellar parameters, the GIRFIT code computes the synthetic spectra from a  $T_{\text{eff}}/\log g$ -interpolation in a grid of fluxes created with the SYNSPEC programme (Hubeny & Lanz 1995, see references therein). To account for additional opacities due to Rayleigh scattering and  $H^{-}$  ions, we enabled the IRSCT and IOPHMI opacity flags of SYNSPEC. All the calculations were performed with ATLAS 9 using LTE atmosphere models computed by Castelli & Kurucz (2003). The microturbulent velocity was supposed to be 2 km s<sup>-1</sup> and a solar-type chemical composition was considered.

**Table 5.** Log of the CCD differential multi-site photometric campaign conducted for HD 217860.

Dates (yr 2005)	Site	Observer(s)	$N_{data}$	C1	K	NSV
<i>Filter B</i>						
Nov. 4 – Dec. 25	UAO	KG	1274	y	y	n
Dec. 3, 2004 – Nov. 22	BHO	PVC, PL	2970	y	y	y
Jun. 13 – Dec. 25	ZO	SK	5667	y	y	n
Dec. 3, 2004 – Dec. 25	All	All	9911	y	y	n
<i>Filter V</i>						
Nov. 4 – Dec. 25	UAO	KG	1130	y	y	n
Jul. 14 – Nov. 22	BHO	PVC, PL	2751	y	y	y
Jul. 5 – Dec. 25	ZO	SK	1599	y	y	n
Jul. 5 – Dec. 25	All	All	5384	y	y	n

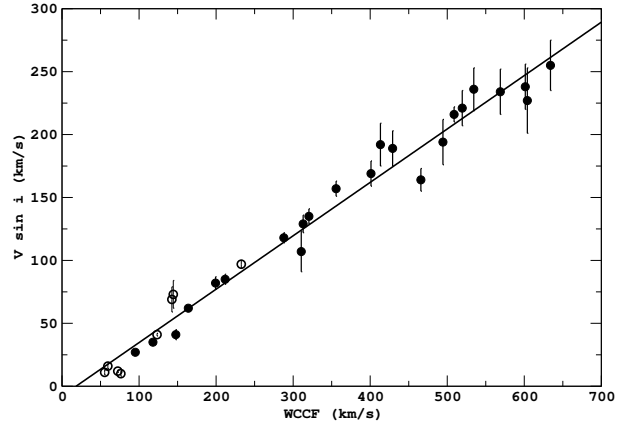
**Fig. 3.** HD 217860 – Comparison between observed (dotted black line) and synthetic spectra (full red line).

The programme SPECTRUM (Gray 2005) as well as the previously mentioned grid of LTE atmosphere models (for a solar-type chemical composition) were used to compute the synthetic spectra for obtaining the additional NAO radial velocities.

## 4. Results

### 4.1. Spectroscopy

The procedure described in Sect. 3 was applied to the spectra of all the targets of our sample. As an example of the agreement we obtained between observed and synthetic spectra, we

**Fig. 4.** Relation between the full base width of the cross-correlation function (WCCF) and the  $V \sin i$  parameter. The linear least squares relation between the measurements made on single-lined objects (filled circles) is represented by the full line.  $V \sin i$  values obtained for components member of multiple systems are also plotted (unfilled circles).

show those of HD 217860 in Fig. 3. The resulting stellar parameters are listed for each target in Table 7: the HD (col. 1) and HIP (col. 2) identification numbers, the effective temperature (col. 3), the surface gravity (col. 4), the projected rotation velocity (col. 5), and the radial velocity (col. 6). Remarks concerning multiplicity, pulsation and/or chemical composition are reported in col. 7. In Fig. 4, the projected rotation velocities of single stars and of single-lined spectroscopic binaries (SB1s) are plotted relative to the full width of the estimated baseline of the CCF (WCCF, see Fig. 2). The linear relation that exists between WCCF and  $V \sin i$  can be used to verify the projected rotation velocity determination of stars belonging to spectroscopically resolved binaries (SB2s).

### 4.2. CCD photometry

Fig. 5 illustrates the light curves obtained in the B or V filter for seven targets: HD 3743 (a new binary), HD 12389 (a known  $\delta$  Scuti star), HD 20194 (a photometrically constant star), HD 68725 (a newly detected  $\delta$  Scuti star), HD 81995 (a new eclipsing binary), HD 217860 (a new multiperiodic  $\delta$  Scuti

**Table 7.** Stellar parameters of the targets. Remarks: "VAR" are the short-term variables; "ell." means ellipsoidal variations are detected in the CCD photometry. The spectra of the 3 framed SB2 targets were analysed accounting for the contribution of two components. Numbers between brackets represent the number of measurements used to compute the average radial velocity (col. 6).

HD	HIP	$T_{\text{eff}}$ [K]	$\log g$	$V \sin i$ [km s <sup>-1</sup> ]	RV [km s <sup>-1</sup> ]	Remarks
849	1043	7714± 285	3.99±0.07	169± 10	7.33± 7.21 (2)	
3066	2719	8149± 450	3.97±0.09	255± 20	-7.26± 5.72 (4)	
3743	3165	7895±3.81	3.81±0.15	97± 3	-8.16± 1.88 (3)	VAR, ell. ?, SB2
3777A	3227A	8242± 180	4.04±0.10	12± 1	34.06± 0.41 (2)	SB2, Am
5066	4129	9336± 246	3.58±0.09	127± 5	-10.45± 5.24 (2)	
6813	5416	$\gamma = 13 \pm 10 \text{ km s}^{-1}$ ; $R_{AB}^I = 4.36 \pm 1.56$				SB2
6813A	5416A	8016± 350		69± 10		
6813B	5416B	8596± 350		10± 2		
7751	5886	8240± 186	3.90±0.10	157± 6	11.21± 6.80 (2)	
11190	8581	$\gamma = 2.30 \pm 0.47 \text{ km s}^{-1}$ ; $R_{AB}^I = 2.02 \pm 0.02$				SB2
11190A	8581A	7519± 150	3.80±0.19	16± 2		Am
11190B	8581B	7416± 230	4.02±0.19	11± 2		Am
12389	9501	8155± 250	3.64±0.20	82± 5	-37.84± 2.00 (2)	known $\delta$ Sct, VAR
12868	9851	8236± 164	3.26±0.21	7±0.6	-3.89± 0.16 (2)	SB1?
13162	10045	9104± 170	3.85±0.18	27± 2	-5.20± 0.37 (2)	
14155	10731	8300± 350	4.19±0.09	234± 18	-11.09±10.32 (2)	VAR
17217	13063	8610± 200	4.13±0.07	216± 6	-9.53± 7.60 (2)	
19257	14479	7367± 195	4.23±0.06	135± 6	0.26± 4.88 (2)	VAR
20194	15177	7702± 200	4.03±0.12	238± 18	-5.98± 6.18 (2)	
25021	18777	8056± 50	3.99±0.10	85± 4	-23.28± 2.36 (2)	Am
26212	19436	7873± 290	4.09±0.10	221± 14	9.67±11.18 (4)	
27464	20495	7470± 175	3.18±0.22	105± 5	-1.30± 3.25 (2)	
30468	22352	9068± 213	3.98±0.10	129± 7	-12.29± 7.25 (3)	
31489	22984	7751± 350	3.91±0.11	236± 17	15.17± 4.41 (2)	
38771	27525	7753± 220	3.28±0.25	79± 5	7.47± 2.71 (2)	
42173	29375	7590± 148	4.09±0.09	194± 18	-2.46± 8.25 (3)	
44372	30287	8386± 400	3.60±0.25	107± 16	12.42± 2.00 (1)	
64934	38891	7849± 371	4.00±0.10	227± 26	-14.67± 5.36 (2)	
68725	40361	7000± 100	3.60±0.11	41± 4	-5.80±6.91 (10)	SB2 ? or/and CP/Am, new $\delta$ Sct, VAR
81995	46642	7868± 144	3.97±0.10	62± 2	24.04± 2.18 (4)	VAR, SB1, eclipsing
217860	113790	7286± 100	3.87±0.05	32± 2	3.58± 2.45 (3)	new $\delta$ Sct, VAR
221774	116321	$\gamma = 13 \pm 5 \text{ km s}^{-1}$ ; $R_{AB}^I = 3.2 \pm 1.2$				SB2
221774A	116321A	8056± 200		41± 1		
221774B	116321B	7132± 400		73± 11		
223425	117479	8712± 268	4.23±0.08	192± 17	1.83± 2.82 (2)	
223672	117646	8015± 237	3.30±0.34	164± 9	8.05± 4.60 (4)	
224624	118276	8439± 256	4.21±0.07	189± 14	-9.34± 1.94 (3)	
225125	300	7631± 235	3.93±0.10	118± 4	-4.70± 2.02 (2)	

star) and HD 221774 (a photometrically constant SB2). The discovery of two new  $\delta$  Scuti variable stars has already been reported elsewhere (Frémat et al. 2005a). We generally used an arbitrary shift to plot the light curves of both the *target minus comparison star* and the *comparison minus check star* in one and the same panel (after having removed the mean difference in magnitude for each data set).

### 4.3. Frequency-analysis for HD 217860

#### 4.3.1. Results

We performed the frequency analyses with the software package PERIOD04 which is based on the classical Fourier analysis

(Lenz & Breger 2005). As a first step, we carried out a frequency search on the B- and the V-time series for each observatory individually. These preliminary runs indicated two common frequencies in each data set. We next merged the data from all three observatories into larger sets of weighted measurements, one for each filter (sets 'B All' and 'V All'). First we computed the respective spectral windows showing the alias features caused by the gap of almost one year ( $\approx 0.003 d^{-1}$ ) and the  $1 d^{-1}$  spacing. The subsequent frequency searches were performed on the weighted data (using the option 'Point Weight') in the interval from 0 to  $35 d^{-1}$  with a frequency step always smaller than  $1.5 \times 10^{-4}$  in B and  $2.5 \times 10^{-4}$  in V. The total time span is 387 days, which corresponds to

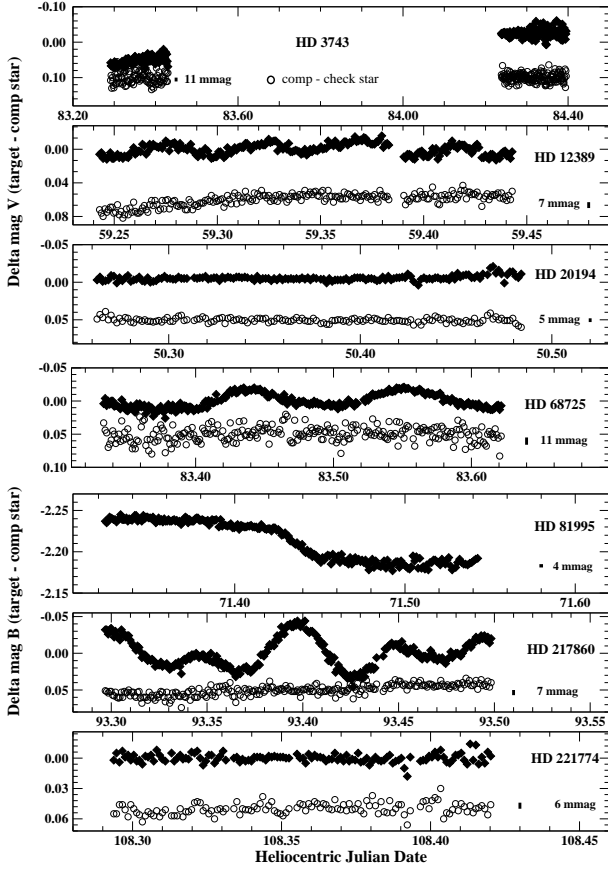


**Fig. 5.** CCD light curves (filter V or B) obtained for seven targets having an obviously variable cross-correlation function. Magnitude differences (i.e target minus comparison star and comparison minus check star) are reported as a function of the Julian date. Arbitrary shifts were applied to present the light curves of the target and comparison data in a single panel. In the case of HD 81995, there was no suitable check star available in the field. Small thick lines show the corresponding standard deviations of the reference data obtained under the best conditions.

$0.0025 d^{-1}$  in frequency, for set 'B All' and 158 days, which corresponds to  $0.0063 d^{-1}$ , for set 'V All'. After each computation, the most dominant frequency was prewhitened from the original (respectively the residual) data in successive steps of the frequency searches. We stopped the analyses when a significance of 4 above the binned noise level (for the amplitude of an adopted frequency) in the periodogram of the residuals was reached or when the incremental variance reduction after a further prewhitening was less than 1%.

The results of the frequency searches performed unto the weighted B- and V-data sets are presented in Tables 8 and 9. In the former, we list the multi-frequency solution derived from a weighted combination of two independent analyses: we mention the identification number of the frequency, the frequency value (weighted mean), the error in frequency (weighted variance of the individual errors computed with PERIOD04), the signal-to-noise ratio (S/N or significance) and the reduction of

the relative variance in two filters:

$$R = 1 - (\sigma_{\text{residual}} / \sigma_{\text{original}})^2. \quad (1)$$

In both cases, we achieved a total reduction of the relative variance of the order of 80-85%. In the latter, we list the amplitude, the phase, and the residual standard deviation as derived from a multi-parameter least-squares fit of sinusoidal functions applied to each time series. We further mention the amplitude ratio  $A_B/A_V$  (col. 8) and the phase difference  $(\Phi_V - \Phi_B)$  (col. 9) with their respective errors. When accurate, such observed values may be compared to a theoretically derived amplitude ratio and phase difference for a possible determination of the spherical harmonic degree  $\ell$  of the pulsations at a given pulsation constant (see Sect. 4.3.3).

This analysis revealed two major frequencies which appear in all our (individual as well as merged) data sets. These frequencies are  $19.747 d^{-1}$  (F1) and  $12.105 d^{-1}$  (F2), with a frequency ratio of 0.613. Their values, amplitudes and phases are well-determined. Six minor frequencies are furthermore common to both searches: these are - in decreasing order of least-squares amplitude in the filter B -  $9.622 d^{-1}$  (F3),  $14.272$  or  $15.275 d^{-1}$  (F4),  $7.911$  or  $8.911 d^{-1}$  (F5),  $8.105$  or  $9.105 d^{-1}$  (F7),  $8.698$  or  $9.868 d^{-1}$  (F8), and finally, the coupling frequency  $31.852 d^{-1}$  ( $S12 = F1 + F2$ ). Though some amplitudes are at the level of a few mmags, all of these frequencies nevertheless appear with a significant S/N. This is also the case of  $31.852 d^{-1}$ , particularly significant in the set 'B All'. The detection of eight common frequencies in both time series lends credibility to their secure identification, except - in some cases - for the daily aliasing.

#### 4.3.2. Confirmation and interpretation

We additionally performed the search for the best multi-frequency solution (in the sense of a full scale least-squares analysis) using a different method. The data collected in both filters B and V, with their respective weights attributed on a night-to-night base, were simultaneously fitted with a same set of frequencies, but with amplitudes and phases different for each filter. It was not feasible to explore the complete frequency space in six or more dimensions, but the region from 8 to  $10 d^{-1}$  was always well covered. A converging six-frequency solution was found with  $F1 = 19.74727 d^{-1}$ ,  $F2 = 12.10489 d^{-1}$ ,  $F3 = 9.62244 d^{-1}$ ,  $F4 = 14.27155 d^{-1}$ ,  $F5 = 8.91111 d^{-1}$  and  $S12 = 31.85223 d^{-1}$ . These frequencies are within the errors identical to the first five frequencies and the sum frequency of the adopted solution based on the weighted averages of the individual frequency-analyses of the B- and V-time series (cf. Table 8). The associated amplitudes and phases are identical to those of Table 9.

It is interesting to compare our frequency-solution with the one based on the HIPPARCOS measurements: although F1 is clearly present in both, the second most dominant frequency (F2) is not. Instead, the next possible frequency was found at  $14.268 d^{-1}$ , which matches extremely well with one of the two probable values for F4. This is unambiguous evidence for amplitude and/or frequency modulation. Because of the possible detection of  $14.272 d^{-1}$  (F4) in the HIPPARCOS measurements,



we gave preference to this frequency in the adopted multi-frequency solution. However, the alternative choice at  $15.275 d^{-1}$  (F4) would not lead to a different frequency-solution than the one listed in Table 8.

One frequency of the B-time series (i.e.  $F6 = 2.000 d^{-1}$ ) has no matching frequency in the V-time series. We therefore consider this frequency as not being caused by a real effect. In general, we would not trust any detection at a frequency below  $4 d^{-1}$  (such as in the case of set 'B All') due to the treatment and the combination of a variety of data sets. We furthermore remark that, though the B-data are more numerous, we obtained a somewhat smaller significance level for the most dominant frequency (F1) with the B-data than with the V-data. However, the opposite is true for all the other frequencies.

Figs. 6 and 7 illustrate both frequency searches. We plotted the Fourier spectrum of the original data followed by those of the residual data after every successive prewhitening. For sets 'B All' and 'V All', we stopped the search after the detection of 8 frequencies. The coupling frequency at  $31.852 d^{-1}$  was not identified as the next highest peak in the periodograms of the residual data sets, but the obvious pattern imitating the spectral window is a clear indication of its unambiguous identification. Since its S/N is at least equal to 3 in both sets, we also included this frequency in the final fitting process.

Two parallel frequency searches performed on the differential magnitudes (K - C1) revealed no significant peaks with an amplitude larger than 1 mmag in both time series. We estimated upper limits for the expected noise level from these data (the differential magnitude is larger than for the variable star): we obtained 9.6 mmag (set 'B All') and 9.0 mmag (set 'V All'). As expected, the final scatters of the residual data appear to be much lower: we obtained 7.5 and 7.4 mmag for the B- and the V-residuals respectively (cf. Table 9). We assume that these values reflect the true noise levels of our merged data sets.

#### 4.3.3. Attempt of mode identification

The atmospheric stellar parameters listed in Table 7 were obtained through spectroscopic synthesis of high S/N and high-resolution spectra. Therefore, the stellar parameters of HD 217860 are known with a relatively good accuracy. This enabled us to compute, together with the frequencies of Table 8, reliable values for the pulsation constant which are useful to attempt identification of the excited modes. The following expression can be used here (Breger 2000):

$$\log Q = -\log f + 0.5 \log g + 0.1 M_{bol} + \log T_{eff} - 6.456,$$

allowing a relative accuracy of about 7% on the pulsation constant. Deriving  $M_{bol} = 1.65 \pm_{0.13}^{0.07}$  from the star's location in the H-R diagram, we obtained the pulsation constants of Table 10. We can see that the two most dominant modes may correspond to radial (overtone) modes, while F3 could possibly be identified as the fundamental radial mode (F). Remark, however, that the corresponding frequency ratio  $F2/F1$  is 0.613 (this value matches the standard ratio expected for 2H/F, Bono et al. 1997).

**Table 8.** Adopted frequency-solution based on the weighted analyses of the sets 'B All' and 'V All'

Freq. Id.	Freq. ( $d^{-1}$ )	Error ( $d^{-1}$ )	S/N	R (%)	S/N	R (%)
			<i>Filter B</i>		<i>Filter V</i>	
F1	19.747258	0.000013	41.4	51	44.6	50
F2	12.104912	0.000019	24.5	75	20.0	71
F3	9.622399	0.000078	8.3	76	7.3	72
F4	14.271621 <sup>a</sup>	0.000059	6.9	79	4.9	73
F5	8.910976 <sup>a</sup>	0.000083	7.6	81	6.9	75
F6	2.000229 <sup>b</sup>	0.000075	5.6	82	—	—
F7	8.69806 <sup>a</sup>	0.00011	5.6	83	6.3	76
F8	8.10529 <sup>a</sup>	0.00012	4.6	84	6.2	78
S12	31.85217	0.00014	6.9	84.6	3.3	78.0

<sup>a</sup>: these values may be affected by the  $1 d^{-1}$  (and  $0.003 d^{-1}$ ) aliasing i.e. 15.275, 9.698 and  $9.105 d^{-1}$  give equally good fits. Preference was given to a solution with 14.272 (since marginally found in the Hipparcos data),  $8.911 d^{-1}$  (peak convincingly detected in 'B All') and  $8.698 d^{-1}$  (peak convincingly detected in 'V All').

<sup>b</sup>: this frequency was not found in 'V All', but there is an insignificant peak at  $2.89$  or  $3.89 d^{-1}$ .

**Table 9.** Amplitude(s) (ratios) and phase(s) (differences) in two filters for the adopted frequency-solution. All the phases are computed with respect to the initial epoch of set 'B All'. The standard errors on the derived parameters are also shown.

Freq. Id.	$A_B$ (mmag)	$\sigma_B$ (mmag)	$\Phi_B$ ( $2\pi$ rad)	$A_V$ (mmag)	$\sigma_V$ (mmag)	$\Phi_V$ ( $2\pi$ rad)	$A_B/A_V$	$\Phi_V - \Phi_B$ ( $2\pi$ rad)
	<i>Filter B (19.0)</i>			<i>Filter V (15.7)</i>				
F1	19.3	13.3	0.39	16.0	11.1	0.40	$1.21 \pm 0.02$	$0.006 \pm 0.003$
F2	13.4	9.5	0.23	10.7	8.5	0.24	$1.25 \pm 0.04$	$0.008 \pm 0.005$
F3	4.3	9.3	0.46	2.7	8.3	0.44	$1.54 \pm 0.16$	$-0.01 \pm 0.02$
F4	4.2	8.8	0.28	2.9	8.1	0.30	$1.34 \pm 0.15$	$+0.01 \pm 0.02$
F5	3.9	8.3	0.60	3.2	7.9	0.59	$1.35 \pm 0.13$	$-0.01 \pm 0.02$
F6	3.6	8.0	0.54	—	—	—	—	—
F7	2.9	7.7	0.56	2.7	7.7	0.53	$1.09 \pm 0.14$	$-0.03 \pm 0.02$
F8	2.4	7.6	0.87	2.7	7.4	0.91	$0.91 \pm 0.12$	$+0.04 \pm 0.02$
S12	1.7	7.5	0.42	1.3	7.4	0.45	$1.3 \pm 0.3$	$+0.03 \pm 0.04$

Additionally, we used the most recently developed models for  $\delta$  Scuti stars including also stellar atmospheres with low-efficiency convection (Montalbán & Dupret 2007) to perform a comparison between the theoretical frequency values of modes with degree  $\ell = 0, 1, 2$  or  $3$  and the observed two most dominant ones. Only for these frequencies, an accurate determination of the amplitudes and phases in B and V is possible. We selected 19 appropriate models of mass 1.80, 1.85 and  $1.90 M_{\odot}$  predicting F1 at a value less than  $0.2 c/d$  from its observed value and whose atmospheric stellar parameters satisfy the conditions in effective temperature and gravity of  $\Delta \log T_{eff} < 0.015$  and  $\Delta \log g < 0.1$ . Then, we looked at those models which

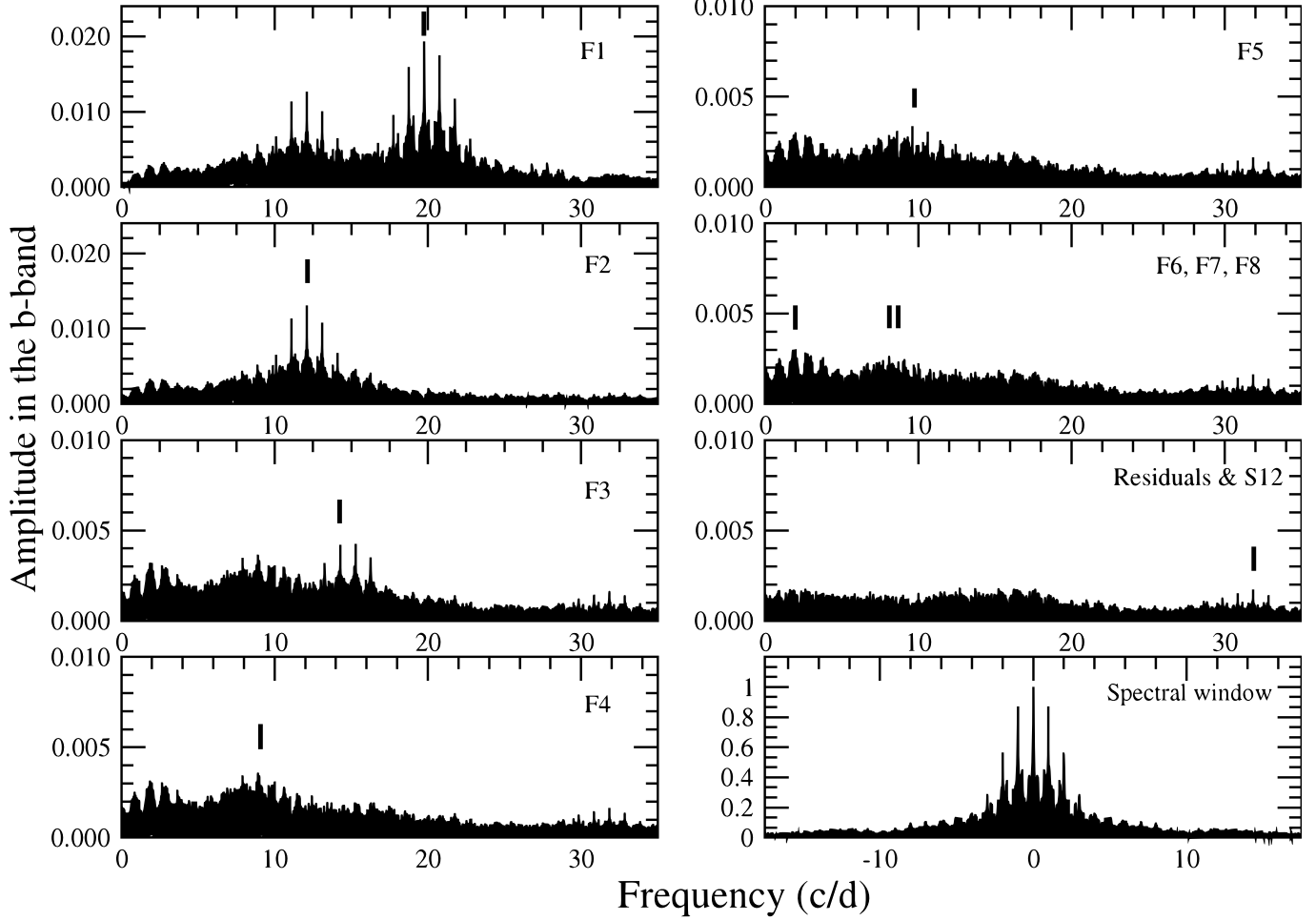


**Fig. 6.** Successive frequency searches and spectral window of the Fourier analysis (Set All - filter B)

**Table 10.** Derived pulsation constants for the frequencies of the adopted solution and possibly corresponding mode identification.

Freq. Id.	Q (days)	$\sigma_Q$ (days)	Mode Id.
F1	0.016(3)	0.001(1)	poss. 3H
F2	0.026(6)	0.001(8)	poss. 1H
F3	0.033(4)	0.002(2)	poss. F
F4	0.022(5)	0.001(5)	poss. 2H
F5	0.036(1)	0.002(4)	non-radial?
F7	0.037(0)	0.002(4)	non-radial?
F8	0.039(7)	0.002(6)	non-radial?

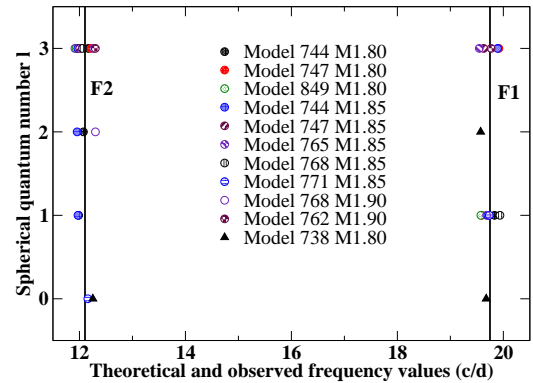


**Fig. 8.** Theoretically predicted versus observed frequencies for F1 and F2. Vertical lines represent the observed frequency values.

also predict F2 at less than 0.2 c/d from its observed value: 10 models remained. Fig. 8 illustrates the differences for F1 and F2 versus the spherical harmonic degree  $\ell$  for the 10 models matching all the requirements. From this comparison, we see that most models indicate non-radial pulsation with  $\ell = 1$  or 3 for F1, and  $\ell = 2$  or 3 for F2. In one such case (model #771 with a mass of  $1.85 M_{\odot}$  and  $\Delta \log T_{\text{eff}} = 0.012$ ), we found a radial mode ( $\ell = 0$ , identified as the first overtone 1H) for F2

and a non-radial one ( $\ell = 1$ ) for F1. In one more model, but a slightly less evolved one lying just outside the range of allowed parameters (model #738 with a mass of  $1.80 M_{\odot}$  and  $\Delta \log g = 0.12$ ), we found excitation of two radial modes: the fundamental radial mode (F) for F2 and the second overtone (2H) for F1 (another but poorer match indicated  $\ell = 2$  for F1) (cf. triangles in Fig 8).

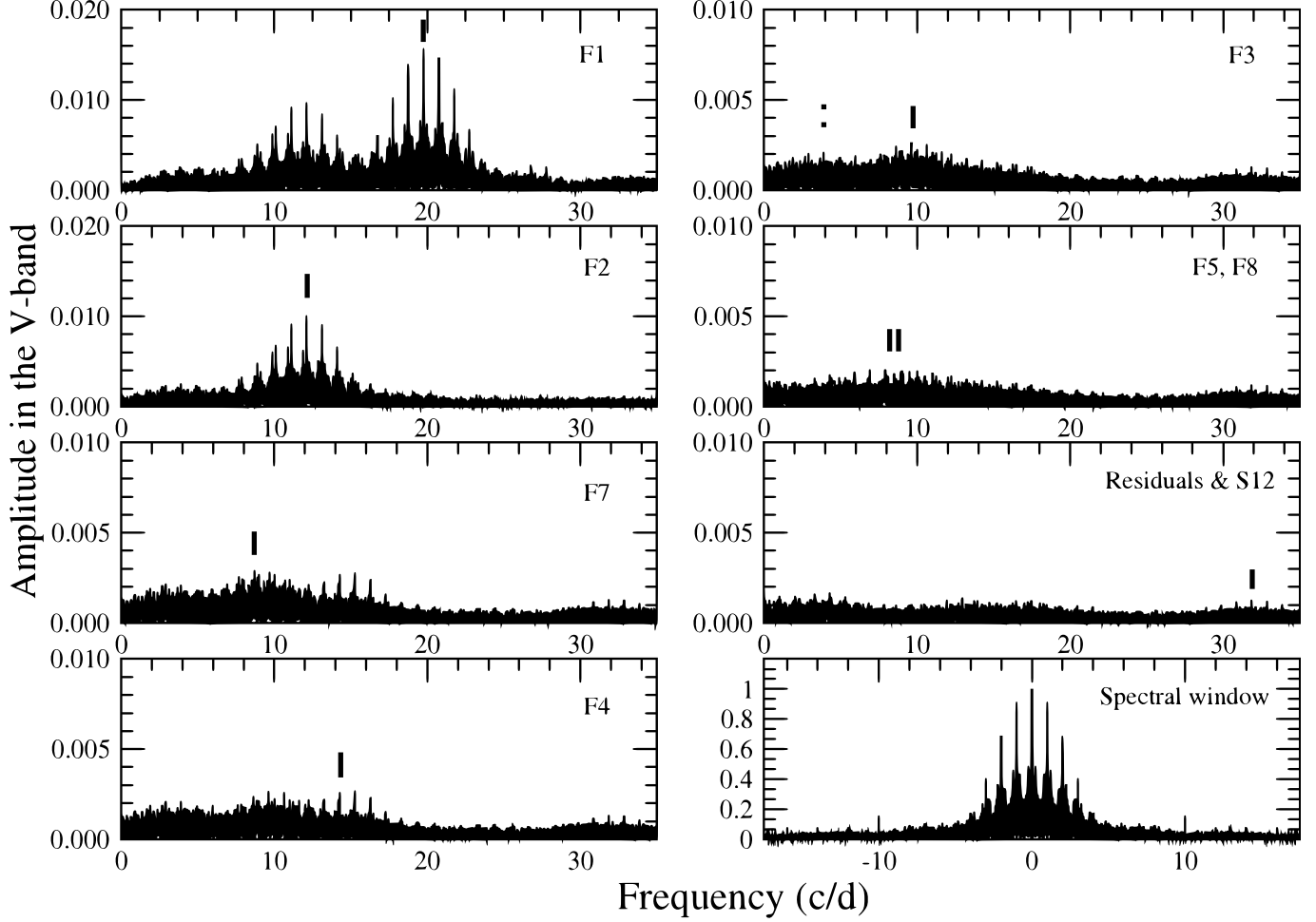


**Fig. 7.** Successive frequency searches and spectral window of the Fourier analysis (Set All - filter V)

Another tool possibly useful for the determination of the spherical harmonic degree  $\ell$  of the pulsations at a given value of the pulsation constant (Garrido 2000; Dupret et al. 2003) is the comparison between observed photometric and theoretical values of the amplitude ratio and the phase difference provided by two-colour photometry. We used the same models as in Fig. 8 to derive the non-adiabatic quantities for the  $\ell = 0, 1, 2$ , and 3 modes. In Fig. 9, we show the resulting amplitude ratio versus phase difference diagramme for the 11 models with frequencies matching both F1 and F2. For each model, the harmonic degree  $\ell$  is represented by a different symbol. The amplitude ratios and the phase differences corresponding to the extra model #738 with a mass of  $1.80 M_{\odot}$  correspond to the filled symbols. Although, as we can see, there is a discrepancy with the predicted amplitude ratios (notwithstanding the inclusion of thin convective zones), the phase differences are in good agreement. We conclude from this diagramme that the observed values (Table 9) might be compatible with low-degree ( $\ell = 0, 1$  or 2) modes while  $\ell = 3$  modes are not probable since the theoretical non-adiabatic observables lie too far from their observed counterparts.

## 5. Remarks on other interesting targets

### 5.1. HD 3743 – HIP 3165

The star is the primary of a visual binary system also known as CCDM 00403+2403 A, forming a common proper motion pair (CPM) with CCDM 00403+2403 B (= HIP 3163) (angular separation =  $16.5''$ , position angle =  $205.5^{\circ}$  and  $\Delta H_p = 2.29$  mag, ESA 1997). Since the circular entrance pupil of the ELODIE fiber is  $2''$  across, only component A was observed. However, the star showed a bottle-shaped CCF. The differential photometric analysis showed a shift of  $0.078$  mag in mean light level between two consecutive nights. Though the scatter is large (about  $0.01$  mag) and increases at the end of each time series (due to higher airmass), the *comparison minus check star* data do not reveal this feature. We therefore suggest that HIP 3165 is a close binary and that the change in mean level could be related to ellipsoidal variations with a periodicity of several days. This behaviour is also confirmed by a simple Fourier analysis of the HIPPARCOS epoch photometric data: a period of  $\sim 320$  days was derived with an amplitude of  $0.02$  mag. The HIPPARCOS sampling is, however, very scarce and much shorter periods are thus possible (and even probable). For all these reasons we propose HD 3743=HIP 3165 as a new SB2, making CCDM 00403+2403 AB at a least triple sys-

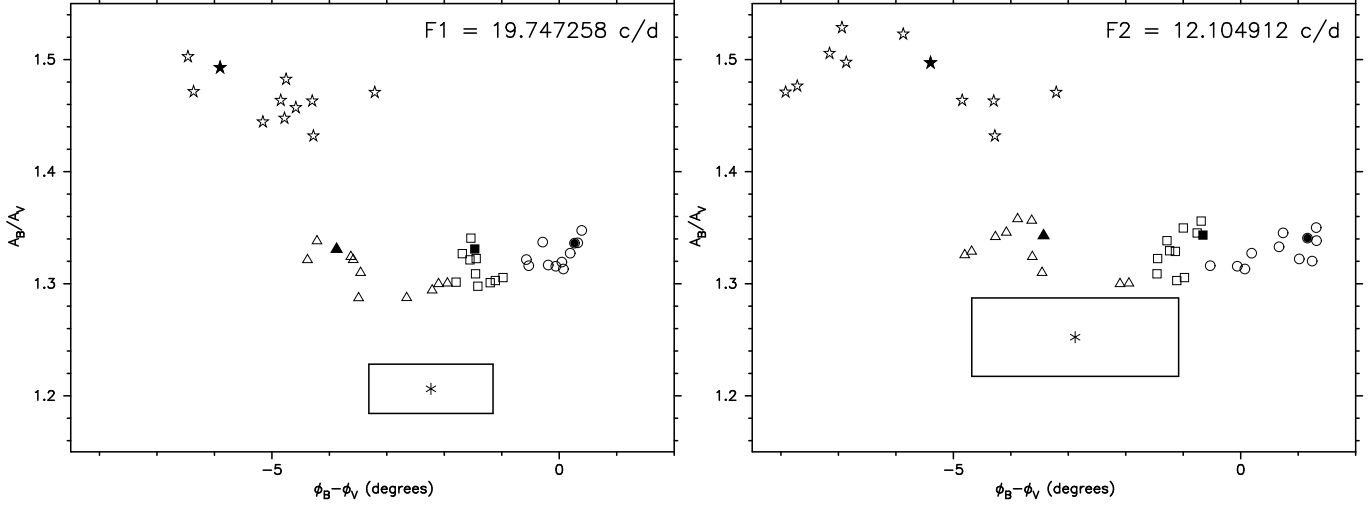


**Fig. 9.** Observed and theoretical values in an (amplitude ratio vs. phase difference) diagram for the  $\ell = 0$  (circles), 1 (squares), 2 (triangles), and 3 (stars) modes whose frequency is the closest to the observed frequencies F1 (left panel) and F2 (right panel) for the 11 selected models of mass 1.80, 1.85, and 1.90  $M_{\odot}$ . The amplitude ratios and the phase differences corresponding to the extra model #738 of mass 1.80  $M_{\odot}$  correspond to the filled symbols. One  $\sigma$ -error boxes are plotted around the observed values.

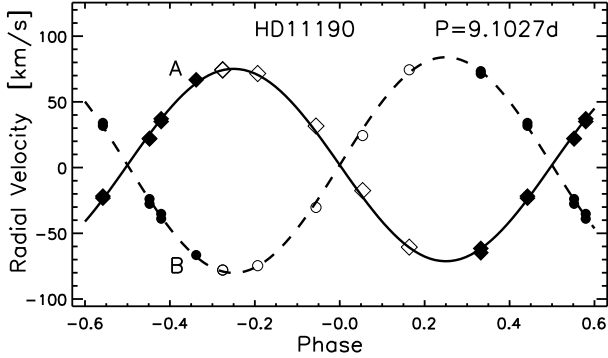


**Fig. 10.** Radial velocity phase diagram of HD 11190. Full and dashed lines represent the orbital solution assuming a circular orbit. Filled symbols correspond to data collected at NAO Rozhen, unfilled ones to data collected at OHP.

tem. However, more differential photometric data are needed in order to confirm this work hypothesis.

### 5.2. HD 3777 – HIP 3227

HD 3777 was classified as an Am star by Bidelman (1964) and by Cowley & Cowley (1965). Bertaud (1970) reported broad and weak metallic lines. The radial velocity of the star varies with an amplitude of about 40  $\text{km s}^{-1}$  (Duflot et al. 1992; Grenier et al. 1999), probably due to binarity, as confirmed by the two peaks detected in the CCFs. However, the secondary is much fainter than its companion and we were able to fit the spectrum assuming only one component. Since the observed Ca II K is fainter than usual, we hereby confirm that this star is a chemically peculiar star of type Am.

### 5.3. HD 11190 – HIP 8581

Very little is known about HD 11190 except for its variable radial velocity. Actually, this star forms a SB2 system consisting of two almost identical components (Fig. 10). We monitored it spectroscopically during five consecutive nights in May 2005 and four nights in December 2006. The orbital parameters we derived from the adjustment of the radial velocity measurements assuming a circular orbit are presented in Table 11.

**Table 11.** Orbital parameters of HD 11190 assuming a circular orbit

$P =$	$9.1027 \pm 0.0002$ days
$T_0 =$	$2453336.907 \pm 0.016$ JD
$K_A =$	$73.19 \pm 0.72$ $\text{km s}^{-1}$
$M_B/M_A =$	$0.892 \pm 0.017$
$\gamma =$	$1.93 \pm 0.35$ $\text{km s}^{-1}$

The fitting of the hydrogen lines provides very similar parameters for the two components and correspond to an A9 IV-V spectral type. Since the Ca II K line of the components is very weak, and would better agree with that of an A3 star, we may conclude that both components are Am stars. The luminosity ratio ( $R_{AB}^L = 2.02 \pm 0.02$ ) and interpolation through theoretical evolutionary tracks further provide:

$$\begin{aligned}
 M_A &= 2.03 \pm 0.19 M_{\odot} \\
 R_A &= 2.97 \pm 0.81 R_{\odot} \\
 R_A/R_B &= 1.39 \pm 0.90.
 \end{aligned}$$

The dynamical mass ratio is in good agreement with the luminosity ratio obtained from spectroscopy and atmosphere modeling. Although the stellar radii are affected by large error bars, it is interesting to note that their ratio is almost equivalent to the ratio of the  $V \sin i$  values ( $1.45 \pm 0.31$ ), which means that the rotation of both components is probably synchronized with the

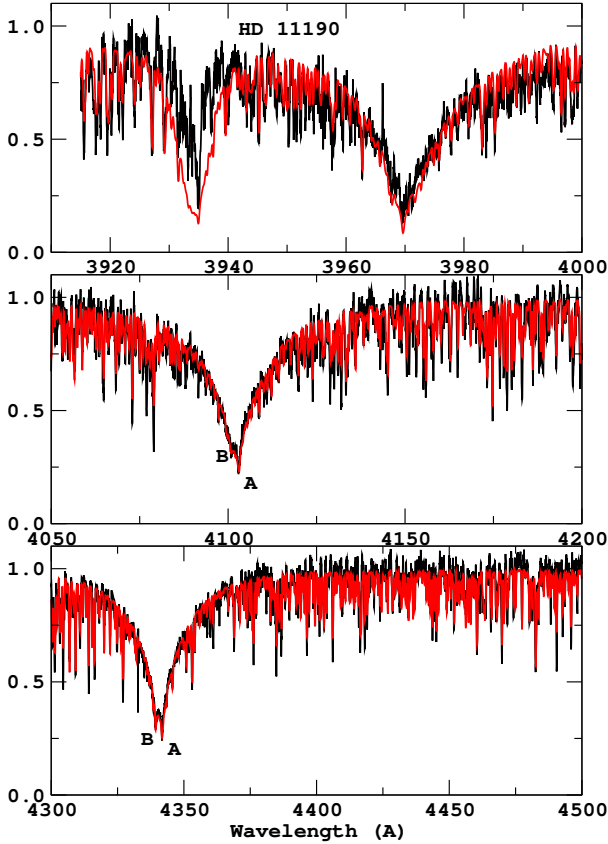


**Fig. 11.** Comparison between observed (black line) and synthetic spectra (red line) in the case of the SB2 system HD 11190 at HJD=2453343.4033. The presence of the two components was taken into account in the fit. The significant disagreement between observations and model indicates that both components are Am stars.

orbital motion. This is also supported by the low  $V \sin i$  values of both components. Assuming that  $i_{\text{spin}} \approx 90^\circ$  and the alignment of the spin and the orbital axes, one would expect values very close to the observed ones:

$$V_{\text{synch.}}^A = 17 \text{ km s}^{-1}, V_{\text{synch.}}^B = 12 \text{ km s}^{-1}.$$

Note, however, that the propagated error bars on these estimates are large (i.e.  $29 \text{ km s}^{-1}$ ), which does not allow us to conclude on the spin/orbit inclination itself.

#### 5.4. HD 12389 – HIP 9501

Colours in the Strömgren photometric system are available for this star from Handler (1995, 1999). Adopting the calibration of Moon & Dworetzky (1985), we found  $T_{\text{eff}} = 8230 \text{ K}$  and  $\log g = 3.87$  (i.e. corresponds to A5 IV), while the spectral types provided by SIMBAD and by Grenier et al. (1999) are A0 and A4 V, respectively. The fitting of the ELODIE data with synthetic spectra results in an effective temperature in good agreement with the one obtained from uvby photometry. The CCF shows clear LPVs. We obtained one light curve on JD 2453359 (cf. Fig. 5). Despite a dip at the beginning of the light curve of the *comparison minus check star*, the data are of very good quality. Though the *star minus comparison*

data show a standard deviation of at most 6 mmag, the presence of regular, short-period and small-amplitude variations is obvious. This star is actually a known  $\delta$  Scuti variable star previously detected by (Schutt 1991). A period of 0.04 day and a total peak-to-peak amplitude of 0.03 mag were reported (Rodríguez et al. 2000). From our data, we estimated a similar period ( $\sim 0.045$  day) and amplitude.

#### 5.5. HD 68725 – HIP 40361

HD 68725 was first recognized as a peculiar Am or Ap star by Olsen (1980) on the basis of Strömgren photometry, then by Abt (1984) who classified it as kF2/hF5/mF6 from  $1 \text{ Å}$  resolution spectra, while Grenier et al. (1999) classified it F2Ib. In the H-R diagram it is located at the cooler edge of the CIS and close to the Terminal Age Main Sequence (TAMS; Fig. 12), rather than being a supergiant star. Chemical peculiarities are found when comparing our data to synthetic spectra. They are mainly visible for the rare earth elements:  $\lambda 4078$ ,  $4215 \text{ Sr II}$  resonance lines are significantly stronger in the observed spectra while the iron peak elements are only marginally stronger. Scandium and calcium are nearly solar. HD 68725 is therefore marginally an Am star, but the enhanced Sr possibly indicates the presence of a magnetic field. In their survey of the Solar neighbourhood, Nordström et al. (2004) reported  $[\text{Fe}/\text{H}] = +0.33$  for this star. Mason et al. (2001) observed it twice using speckle-interferometry but found no evidence for multiplicity. However, the night-averaged CCF shows a slight and systematic bump on the left side of the main peak which could be related to the presence of a secondary component. This seems to be confirmed when comparing the averaged radial velocity we obtained ( $RV = -6.9 \pm 4.1 \text{ km s}^{-1}$ ) to the ones previously published by Duflot et al. (1990,  $-36 \pm 0.8 \text{ km s}^{-1}$ ), Grenier et al. (1999,  $-17.5 \pm 5.6 \text{ km s}^{-1}$ ) and Nordström et al. (2004,  $-10.9 \pm 1.1 \text{ km s}^{-1}$ ). It is worth mentioning that, we cannot exclude at the present time that this bump could also be due to a spot, which could provide another proof of an existing magnetic field.

The CCF of HD 68725 further shows rapid shape changes (Fig. 2), probably caused by pulsation of the  $\delta$  Scuti-type as we indeed detected short-period variations in the CCD photometric data. The light curve in Fig. 5 suggests a period of  $\sim 0.12$  days. HD 68725 is therefore a chemically peculiar star which also does pulsate as a typical  $\delta$  Scuti star. More spectra are however needed to decide whether it is a mild Am or a Ap star. If it would prove to be a magnetic Ap star (showing magnetic variations along with spectral variations modulated by the rotational period), it would be an exceptional case, together with HD 75425, a weak Ap Sr(CrEu) star (Martinez & Medupe 1998) and HD 188136, a  $\rho$  Pup star (Kurtz 1980). Such cases suggest that the presence of a global magnetic field does not inhibit  $\delta$  Scuti pulsation in all cases (in contradiction with the actual knowledge of the diffusion theory, see Kurtz & Martinez 2000).

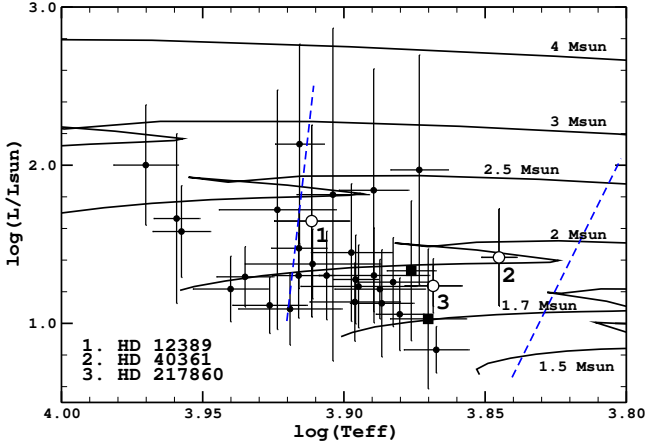


**Fig. 12.** Location of the targets in the H-R diagram. Open circles are the stars we identified as short-term variables of  $\delta$  Scuti type. Squares stand for the components of the SB2 binary HD 11190. Other SB2 systems with inaccurate parameters were not plotted here. Broken lines are the limits of the Cepheid instability strip as computed by Dupret et al. (2005)

### 5.6. HD 81995 – HIP 46642

The HIPPARCOS Epoch photometry of HD 81995 varies with time in an unclear way (unsolved HIPPARCOS variable). The CCF is affected by short-term LPVs and by radial velocity variations due to the presence of a much fainter companion. The star is therefore SB1. We additionally obtained two light curves on JD 2453462 and JD 2453471. Both time series show a partial eclipse, with a drop in magnitude of about 0.06 mag. The standard deviations on the *comparison minus check star* data are 5 and 7 mmag respectively. The light curves are typical of a detached or semi-detached binary (Fig. 5). A third light curve obtained on JD 2453472 showed no changes and a standard deviation of only 4 mmag. In the latter time series, the comparison star appeared to be unreliable.

### 5.7. HD 221774 – HIP 116321

HD 221774 was found to be a double-lined spectroscopic binary in which the primary and the secondary components have spectral types A6 and F1, respectively. Small changes were detected in the high S/N CCFs of this binary. We therefore observed it photometrically for two partial nights. Both *star minus comparison* time series have a standard deviation of 4 mmag and do not show any detectable sign of short-period variability, while the standard deviation of *comparison minus check star* data was 6 mmag. The light curve in Fig. 5 illustrates the data obtained on JD 2453408. We thus classified HD 221774 as a photometrically constant star.

## 6. Discussion and conclusions

We obtained several high-resolution, high signal-to-noise spectra distributed over various time scales ranging from a couple of hours to some days for a sample of 32 bright though poorly investigated A-type stars selected on the basis of their variable

**Table 12.** List of interesting targets

HIP	Remarks
Intrinsically variable stars	
9501	known $\delta$ Scuti
40361	SB2? or/and CP/Am star
113790	$\delta$ Scuti, multiperiodic
Spectroscopic systems	
3165	SB2, ellipsoidal?
3227	SB2, Am star
5416	SB2
8581	SB2
9851	SB1?
40361	SB2, CP/Am star
81995	SB1, eclipsing
116321	SB2

radial velocity (Grenier et al. 1999). These spectra were supplemented by differential CCD light curves collected as time series during parts of at least two nights in seven cases, in order to look for rapid light variations. Among the 32 investigated targets, we discovered eight spectroscopic binaries, one of which is a close (photometric) binary (HD 81995). In one case, we claim the detection of ellipsoidal variability caused by the proximity of both components (HD 3165). In all the cases, the components have projected rotational velocities below  $100 \text{ km s}^{-1}$ , which can be expected if spin-orbit synchronization already occurred. We suggest this state explicitly in the case of the newly detected SB2 (HD 11190), a twin system consisting of two similar components orbiting around one another with a period of 9.1 days. If we except HD 13162, HD 25021 (Am star), HD 38771 and HD 217860 (a pulsating star), all remaining targets have large  $V \sin i$  values associated to broad CCFs (duplicity or multiplicity is not easily detectable in these stars, therefore the high scatter in the previous radial velocity measurements can be misleading and should not be interpreted as an indication of variability or multiplicity 'per se').

Among the 32 investigated targets, we also discovered three small-amplitude  $\delta$  Scuti pulsators showing short-term line-profile variations (LPVs), an outcome confirmed by their CCD differential light curves: one is the already known  $\delta$  Scuti star HD 12389 (Schutt 1991), the other two are newly identified  $\delta$  Scuti variable stars (HD 68725 and HD 217860). The former one (HD 68725) is also a member of a marginally metal-enhanced spectroscopic binary showing strong strontium absorption lines, making it the most intriguing system of our sample.

Because both the spectra and the light curves of the pulsating star HD 217860 displayed a highly multiperiodic behaviour, we organised an extensive photometric campaign for this object during the winter of 2005. Observations using the Bessell filters B and V were gathered at three different sites. The independent analyses of two data sets (the sets 'B All' and 'V All') enabled us to identify eight frequencies common to both time series. The adopted solution was confirmed by a simultaneous multi-frequency search of the joint B- and V-data

sets. The two most dominant frequencies detected show a ratio of 0.61; this accurately determined ratio matches extremely well the standard value expected for 2H/F. However, this ratio appears to be also compatible with the computation of the respective pulsation constants ( $Q_1 = 0.016$  and  $Q_2 = 0.027$  days), which rather indicate 3H/1H (with a theoretical period ratio of 0.60). As a next step, we computed theoretical versus observed frequency differences using 19 appropriate models of mass 1.80, 1.85 and 1.90  $M_{\odot}$ , including convection modelling in the outer layers (Montalbán & Dupret 2007). We performed a comparison between the observed amplitude ratios and phase differences for F1 and F2 on the one hand and their theoretical counterparts on the other hand for 11 models predicting frequencies close to F1 and F2 for  $\ell = 0, 1, 2$ , or 3 modes. From this amplitude ratio versus phase difference diagramme, we concluded that non-radial modes with  $\ell = 3$  are not probable. We also showed that most models indicate non-radial pulsation modes with  $\ell = 1$  for F1, and  $\ell = 2$  for F2. However, there exists one model satisfying the derived stellar parameters for HD 217860 and predicting a radial mode for F2 (as the first overtone, 1H). In addition, we found a less evolved 1.80  $M_{\odot}$  model (lying just outside of the range of allowed stellar parameters with  $\Delta \log g = 0.12$ ), which is consistent with the conclusion that both frequencies might correspond to radial modes, with the second overtone ( $\ell = 0, 2H$ ) and the fundamental ( $\ell = 0, F$ ) modes being excited. Our conclusion is that some of the models in the right location of the H-R diagram predict pulsation in at least one radial overtone mode among the two major frequencies. Among the remaining frequencies with almost equally small amplitudes, the presence of non-radial (mixed) modes is very probable, but we cannot exclude that another radial mode may co-exist (e.g. the frequency F3 with  $Q_3 = 0.033$  days).

We also detected - though at the limit of the allowed significance level - a high-frequency component at  $31.852 d^{-1}$  (or period of about 45 min), corresponding to the coupling frequency F1+F2.

More importantly perhaps, we found clear evidence for a strong modulation of the amplitude(s) and/or (radial) frequency content in this star since a frequency-analysis of the HIPPARCOS Epoch Photometry did not reveal the presence of the frequency that we could identify as the possible first radial overtone (F2). It is possible that this  $\delta$  Scuti star is a radial overtone pulsator with a variable (radial) modal content. For this reason, it is an important case study for the comparison with models of pulsational stability in the middle of the  $\delta$  Scuti instability strip (Bono et al. 1997). Another, recently investigated, multiperiodic  $\delta$  Scuti star shows a very similar behaviour: AN Lyn is an atypical  $\delta$  Scuti star showing peculiar and highly multiperiodic light curves such as HD 217860, for which three independent frequencies (10.1756, 18.1309 and  $9.5598 d^{-1}$ ) were determined (Rodríguez et al. 1997). Changes in amplitude on a long time scale are confirmed for its main frequency (Zhou 2002). Furthermore, Montalbán & Dupret (2007) concluded on the basis of a comparison between observed and theoretical values of the amplitude ratio and the phase difference that radial (overtone) modes are most probably excited.

Given the circumstances and the data, we cannot extract more information for this target at present, but the present results amply illustrate that new high-quality time series of differential data organised at a later date would be very worthwhile in order to accurately determine the full frequency content as well as its time-dependent behaviour. A follow-up spectroscopic campaign would be needed to put additional constraints on the mode identification and to enable an in-depth study of the pulsations of this new and atypical  $\delta$  Scuti pulsator.

Our future work will be to analyse and further exploit the high-resolution spectra obtained here in the context of a broad study of the chemical composition of (poorly studied) main-sequence stars located in the lower end of the Cepheid instability strip, with the main objective to investigate the possible connection(s) between pulsation, radiative diffusion and multiplicity in this intriguing part of the H-R diagram.

**Acknowledgements.** We acknowledge funding from the Belgian Federal Science Policy in the framework of the projects "Modern Aspects of Theoretical and Observational (ground-based and spaceborne) Astrophysics" (Ref. IAP P5/36) and "Pulsation, chemical composition and multiplicity in main-sequence A- and F-type stars" (Ref. MO/33/018). DD is grateful to Dr. Z. Kraicheva for many useful discussions and suggestions. This research is based on data obtained at the *Observatoire de Haute-Provence*, the *Observatoire du Pic du Midi* (France), the Hoher List Observatory (Germany) as well as the NAO Rozhen, operated by the Institute of Astronomy, Bulgarian Academy of Sciences (Bulgaria). We acknowledge the support of the Belgian Science Policy and the Bulgarian Academy of Sciences via bilateral project "Photometric and spectroscopic follow-up studies of binary systems of special interest". The spectroscopic campaigns were funded by the Optical Infrared Coordination network (OPTICON) supported by the Research Infrastructures Programme of the European Commission. We kindly thank Drs. Hubeny and Lanz for making their computer codes available. We furthermore thank Dr. K. Reif, director of the Hoher List Observatory from the AIfA (Argelander Institute for Astronomy, University of Bonn), for the allocated telescope time. Part of the photometric data were acquired with equipment purchased thanks to a research fund financed by the Belgian National Lottery (1999). The referees made various useful suggestions which are gratefully appreciated. This research also made use of the SIMBAD database, operated at the *Centre de Données Stellaires* (Strasbourg, France).

## References

- Abt H.A., Oct. 1984, ApJ, 285, 247
- Baranne A., Queloz D., Mayor M., et al., Oct. 1996, A&AS, 119, 373
- Berry R., Burnell J., 2005, The handbook of astronomical image processing, The handbook of astronomical image processing, 2nd ed., by R. Berry and J. Burnell. xxviii, 684 p., 1 CD-ROM (incl. Astronomical Image Processing Software AIP4WIN, v.2.0). Richmond, VA: Willmann-Bell, 2005
- Bertaud C., Jan. 1970, A&AS, 1, 7
- Bessell M.S., 1995, CCD Astronomy, 2, 20
- Bidelman W., 1964, ONR Symposium held at Flagstaff, Arizona (see reference in Cowley & Cowley 1965)
- Bono G., Caputo F., Cassisi S., et al., Mar. 1997, ApJ, 477, 346



- Breger M., 2000, In: Breger M., Montgomery M. (eds.) *Delta Scuti and Related Stars*, vol. 210 of *Astronomical Society of the Pacific Conference Series*, 3–+
- Castelli F., Kurucz R.L., 2003, In: *IAU Symposium*, 20P
- Cowley A.P., Cowley C.R., Jun. 1965, *PASP*, 77, 184
- Donati J.F., Semel M., Carter B.D., Rees D.E., Collier Cameron A., Nov. 1997, *MNRAS*, 291, 658
- Donati J.F., Catala C., Wade G.A., et al., Jan. 1999, *A&AS*, 134, 149
- Duflot M., Mannone C., Genty V., Fehrenbach C., May 1990, *A&AS*, 83, 251
- Duflot M., Fehrenbach C., Mannone C., Burnage R., Genty V., Sep. 1992, *A&AS*, 94, 479
- Dupret M.A., De Ridder J., De Cat P., et al., Feb. 2003, *A&A*, 398, 677
- Dupret M.A., Grigahcène A., Garrido R., Gabriel M., Scuflaire R., Jun. 2005, *A&A*, 435, 927
- Dworetzky M.M., Dec. 2004, In: *The A-Star Puzzle*, *IAU Symposium*, No. 224, 499–504
- Erspamer D., North P., Jan. 2002, *A&A*, 383, 227
- Erspamer D., North P., Feb. 2003, *A&A*, 398, 1121
- ESA, Feb. 1997, *The Hipparcos and Tycho Catalogues*, ESA SP-1200
- Frémat Y., Lampens P., Van Cauteren P., Robertson C.W., Jun. 2005a, *Communications in Asteroseismology*, 146, 6
- Frémat Y., Neiner C., Hubert A.M., et al., Sep. 2005b, *A&A*, in press, arXiv:astro-ph/0509336
- Frémat Y., Antonova A., Damerdjy Y., et al., Dec. 2006, *Communications in Asteroseismology*, 148, 77
- Garrido R., 2000, In: Breger M., Montgomery M. (eds.) *Delta Scuti and Related Stars*, vol. 210 of *Astronomical Society of the Pacific Conference Series*, 67–+
- Gray R., 2005, <http://www.phys.appstate.edu/spectrum/spectrum.html>
- Grenier S., Baylac M.O., Rolland L., et al., Jun. 1999, *A&AS*, 137, 451
- Handler G., Jun. 1995, *Information Bulletin on Variable Stars*, 4216, 1
- Handler G., Dec. 1999, *Information Bulletin on Variable Stars*, 4817, 1
- Hubeny I., Lanz T., Feb. 1995, *ApJ*, 439, 875
- Kurtz D.W., Oct. 1980, *MNRAS*, 193, 51
- Kurtz D.W., Martinez P., 2000, *Baltic Astronomy*, 9, 253
- Lenz P., Breger M., Jun. 2005, *Communications in Asteroseismology*, 146, 53
- Martinez P., Medupe R., 1998, *Ap&SS*, 259, 57
- Mason B.D., Hartkopf W.I., Holdenried E.R., Rafferty T.J., Jun. 2001, *AJ*, 121, 3224
- Montalbán J., Dupret M., Mar. 2007, *ArXiv Astrophysics e-prints*
- Moon T.T., Dworetzky M.M., Nov. 1985, *MNRAS*, 217, 305
- Neiner C., Henrichs H.F., Floquet M., et al., Dec. 2003, *A&A*, 411, 565
- Nordström B., Mayor M., Andersen J., et al., May 2004, *A&A*, 418, 989
- Olsen E.H., Feb. 1980, *A&AS*, 39, 205
- Rodríguez E., González-Bedolla S.F., Rolland A., et al., Dec. 1997, *A&A*, 328, 235
- Rodríguez E., López-González M.J., López de Coca P., Jun. 2000, *A&AS*, 144, 469
- Schaller G., Schaerer D., Meynet G., Maeder A., Dec. 1992, *A&AS*, 96, 269
- Schutt R.L., Jun. 1991, *AJ*, 101, 2177
- Zhou A.Y., Apr. 2002, *A&A*, 385, 503



# Online Material

**Table 2.** Journal of spectroscopic observations at NAO, OHP and TBL.

HD	HJD-2400000	S/N	exp. [s]	RV [km s <sup>-1</sup> ]	Obs.
849	53346.2338	137	1200	10.46±5.93	OHP
	53346.2493	143	1200	5.17±4.10	OHP
3066	53343.3515	59	644	-12.15±1.35	OHP
	53343.3818	70	1200	-1.75±2.86	OHP
	53344.3245	104	1200	2.68±4.17	OHP
	53344.3399	104	1200	-8.86±2.30	OHP
3743	53346.2782	136	1200	-8.10±0.69	OHP
	53346.2937	135	1200	-8.68±1.73	OHP
	53346.3092	136	1200	-8.10±0.27	OHP
	53723.2489	60	400	-10.07±5.73	TBL
	53723.2541	57	400	-11.04±0.61	TBL
	53723.2593	71	400	-14.07±1.28	TBL
	53723.2645	74	400	-10.11±1.26	TBL
3777A	53346.3278	120	1200	34.12±0.21	OHP
B				-102.83±0.67	
A	53346.3433	105	1200	33.97±0.35	OHP
B				-102.13±0.67	
5066	53344.3869	111	900	-9.39±4.46	OHP
	53344.3988	108	900	-11.11±2.76	OHP
6813A	53346.3709	86	1200	12.33±0.50	OHP
B				3.83±0.50	
A	53346.3864	79	1200	12.32± 0.5	OHP
B				3.27±0.50	
A	53723.2745	65	400	13.95±0.40	TBL
B				6.22±0.87	
A	53723.2797	52	400	13.55±0.42	TBL
B				5.28±1.90	
A	53723.2849	60	400	13.57±0.51	TBL
B				5.23±0.24	
A	53723.2902	55	400	14.36±0.38	TBL
B				6.76±0.41	
7551	53344.3577	84	720	10.32±4.34	OHP
	53344.3676	73	720	12.29±5.23	OHP
11190A	53343.4033	79	1200	74.10±0.50	OHP
B				-77.91±0.48	
A	53343.4188	77	1200	74.55±0.62	OHP
B				-77.99±0.48	
A	53344.2401	75	1200	71.54±0.71	OHP
B				-74.64±0.63	
A	53345.4048	71	1200	31.61±0.45	OHP
B				-30.32±0.20	
A	53346.4068	84	1200	-17.51±0.53	OHP
B				24.37±0.43	
A	53347.5432	28	1200	-60.52±0.35	OHP
B				74.41±0.35	
A	54077.2242	161	900	-61.53 1.15	NAO
B				73.39 3.07	
A	54077.2397	124	1200	-64.77 1.28	NAO
B				71.35 3.03	
A	54078.2333	215	1200	-21.72 2.88	NAO

... continued on next page

HD	HJD-2400000	S/N	exp. [s]	RV [km s <sup>-1</sup> ]		Obs.
B				34.00	4.25	
A	54078.2518	149	1500	-23.25	1.34	NAO
B				31.73	3.95	
A	54079.2205	211	1200	21.83	2.43	NAO
B				-23.88	4.15	
A	54079.2366	134	1200	22.23	2.20	NAO
B				-27.59	4.61	
A	54079.4801	172	1200	37.09	2.81	NAO
B				-35.21	5.19	
A	54079.4959	93	1200	35.05	2.42	NAO
B				-38.94	4.27	
A	54080.2300	50	1200	66.77	2.76	NAO
B				-66.53	5.03	
12389	53346.4230	82	1200	-37.54±	1.06	OHP
	53346.4384	81	1200	-38.32±	1.70	OHP
12868	53343.4364	92	1200	-3.98±	0.13	OHP
	53343.4518	104	1200	-3.85±	0.09	OHP
13162	53346.4544	68	1200	-5.53±	0.33	OHP
	53346.4729	70	1200	-5.04±	0.16	OHP
14155	53345.4242	84	1200	-14.62±	8.06	OHP
	53345.4397	70	1200	-7.55±	6.44	OHP
17217	53344.4147	88	900	-9.84±	2.08	OHP
	53344.4266	78	900	-8.42±	7.31	OHP
19257	53345.4570	81	1200	2.76±	3.74	OHP
	53345.4725	90	1200	-1.83±	3.14	OHP
20194	53344.4442	61	1200	-6.54±	2.91	OHP
	53344.4597	61	1200	-4.94±	5.45	OHP
25021	53346.4909	96	1200	-21.92±	1.95	OHP
	53346.5064	99	1200	-24.64±	1.33	OHP
26212	53343.5295	71	1200	13.71±	6.80	OHP
	53343.5450	84	1200	8.98±	4.00	OHP
	53344.4772	70	1200	9.92±	7.21	OHP
	53344.4926	61	1200	8.17±	3.27	OHP
27464	53343.5621	72	1200	-1.76±	2.74	OHP
	53343.5775	54	1200	-1.00±	1.74	OHP
30468	53343.5984	83	1200	-13.75±	2.27	OHP
	53343.6141	88	1200	-12.52±	4.46	OHP
	53346.5223	67	600	-8.64±	5.24	OHP
31489	53346.5353	67	1200	18.24±	3.60	OHP
	53346.5506	71	1200	13.00±	2.55	OHP
38731	53343.6343	61	1500	7.76±	2.31	OHP
	53343.6531	57	1500	7.29±	1.41	OHP
42173	53344.6047	55	1200	3.69±	4.00	OHP
	53344.6201	66	1200	-0.83±	4.00	OHP
	53345.6505	50	1200	-3.07±	6.00	OHP
44372	53346.6125	34	153	12.42±	2.00	OHP
64934	53345.6157	68	1200	-17.26±	2.00	OHP
	53345.6312	75	1200	-8.20±	5.00	OHP
	53716.6955	65	400	-7.77±	10.64	TBL
	53716.7008	71	400	-19.38±	3.95	TBL
	53716.7060	77	400	-15.92±	9.65	TBL
	53716.7112	70	400	-24.16±	14.18	TBL

... continued on next page

HD	HJD-2400000	S/N	exp. [s]	RV [km s <sup>-1</sup> ]	Obs.
68725	53344.6354	51	1200	-3.49±0.52	OHP
	53344.6509	79	1200	-5.32±0.94	OHP
	53344.6663	84	1200	-8.21±1.23	OHP
	53344.6818	86	1200	-9.01±0.81	OHP
	53345.5106	63	900	-3.93±2.01	OHP
	53345.5225	75	900	-3.84±1.51	OHP
	53345.5345	73	900	-3.62±2.05	OHP
	53345.5465	62	900	-4.19±1.05	OHP
	53345.5584	61	900	-13.84±4.05	OHP
	53345.5710	79	900	-13.60±4.15	OHP
	54078.6139	127	600	-13.36±1.66	NAO
	54078.6234	156	900	-13.96±1.67	NAO
	54078.6345	210	600	-07.85±1.71	NAO
	54078.6422	195	600	-07.63±1.59	NAO
	54079.6026	113	600	-15.93±1.42	NAO
	54079.6116	131	900	-17.41±1.52	NAO
	54079.6238	212	900	-10.65±1.97	NAO
	54079.6336	172	600	-10.77±1.88	NAO
	54079.6438	200	900	-12.19±2.44	NAO
81995	53344.7008	87	1200	23.00±1.54	OHP
	53345.6757	70	1200	23.44±0.15	OHP
	53345.6911	65	1200	25.21±0.66	OHP
	53345.7065	72	1200	28.13±1.89	OHP
	53716.6701	53	400	-17.93±2.02	TBL
	53716.6754	47	400	-18.95±2.11	TBL
	53716.6806	59	400	-20.56±0.29	TBL
	53716.6858	51	400	-20.40±0.91	TBL
	53720.6881	52	400	30.93±3.53	TBL
	53720.6934	41	400	31.18±1.48	TBL
	53720.6985	41	400	31.83±1.00	TBL
	53720.7038	53	400	33.61±1.89	TBL
217860	53343.2347	108	1200	2.06±0.93	OHP
	53343.2512	96	1200	6.14±1.82	OHP
	53343.2695	105	1200	3.89±1.35	OHP
221774A	53345.2348	98	1200	21.51±0.38	OHP
B				-52.74±0.55	
A	53345.2502	113	1200	20.33±0.37	OHP
B				-56.22±0.24	
A	53345.2657	105	1200	20.90±0.40	OHP
B				-52.80±1.80	
A	53345.3485	63	600	20.71±0.53	OHP
B				-54.68±0.41	
A	53346.2635	83	600	13.57±1.00	OHP
B				-58.55±1.66	
A	53572.5836	95	500	-46.01±0.43	TBL
B				52.72±1.96	
A	53572.5900	71	500	-46.75±0.43	TBL
B				50.37±1.96	
A	53572.5963	83	500	-46.14±0.43	TBL
B				51.14±1.96	
A	53572.6027	85	500	-45.87±0.43	TBL
B				49.71±1.96	

... continued on next page

HD	HJD–2400000	S/N	exp. [s]	RV [km s <sup>–1</sup> ]	Obs.
223425	53345.2846	114	1200	4.61± 2.5	OHP
	53345.3001	112	1200	0.37±1.31	OHP
223672	53344.2582	95	1200	8.74±1.80	OHP
	53344.2736	102	1200	9.09±1.80	OHP
	53345.3184	118	1200	7.79±2.07	OHP
	53345.3343	108	1200	5.37±3.22	OHP
	53572.6142	78	500	7.66±4.50	TBL
	53572.6206	77	500	3.73±3.28	TBL
	53572.6269	83	500	5.47±4.13	TBL
	53572.6333	74	500	2.79±2.40	TBL
224624	53345.3627	96	1200	–9.87±1.15	OHP
	53345.3781	83	1200	–9.148±1.20	OHP
	53346.3556	62	600	–8.993±1.00	OHP
	53573.4507	64	500	–6.49±3.52	TBL
	53573.4571	68	500	4.65±7.15	TBL
	53573.4635	71	500	–0.81±4.85	TBL
	53573.4699	65	500	–6.91±3.35	TBL
	53344.2914	89	1200	–3.25±1.60	OHP
225125	53344.3068	93	1200	–5.83±1.24	OHP